THE ASTROPHYSICAL JOURNAL, 492:761–766, 1998 January 10

ASCA OBSERVATION OF A LONG-DURATION X-RAY FLARE FROM THE W UMa–TYPE BINARY VW CEPHEI

C. S. CHOI
Korea Astronomy Observatory, 36-1 Hwaam, Yusong, Taejon 305-348, Korea; cschoi@hanul.issa.re.kr
AND
T. DOTANI
Institute of Space and Astronautical Science, 3-1-1 Yoshinodai, Sagamihara, Kanagawa 229, Japan; dotani@astro.isas.ac.jp
Received 1997 June 13; accepted 1997 August 22

ABSTRACT

We analyze X-ray archive data of the W UMa–type binary VW Cephei taken with *ASCA* on 1993 November 5–6. By analyzing the light curve, we find a long-duration flare of ≈ 7.5 hr with a peak luminosity of 1.2×10^{30} ergs s^{-1} (0.4–3.0 keV) for the assumed distance of 23.2 pc. A flux dip is detected in the light curve at the orbital phase of ~ 0.5, and it is identified as an eclipse by the secondary star. We determine the timescale of the eclipse egress to be ~ 30 minutes from a model fit to the light curve. With this timescale, we estimate that the linear size of the flaring region is $\approx 5.5 \times 10^{10}$ cm, regardless of the flare models. From the spectral analysis of the data, we find that the spectrum can be well reproduced by the variable-abundance plasma model with a combination of two different temperatures, $kT = 0.64$ and $kT = 1.91$ keV. The hotter component is considered to be associated with the flare. The results are interpreted in terms of a two-ribbon flare model, in which we also discuss the possible enhancement of element abundances.

Subject headings: binaries: close — stars: coronae — stars: individual (VW Cephei) — X-rays: stars

1. INTRODUCTION

Since the first detection of X-ray emission from VW Cephei with *HEAO 1* (Carroll et al. 1980), W Ursae Majoris binaries have been observed by many X-ray satellites: *Einstein* (Cruddace & Dupree 1984), *EXOSAT* (Vilhu & Heise 1986), *Ginga* (Tsuru et al. 1992), and *ROSAT* (McGale, Pye, & Hodgkin 1996). W UMa–type binaries, which consist of stars with late spectral types of F–K, are characterized by showing continuous variations of flux during short orbital periods of $P_{\rm orb} = 0.2$–0.8 days (for a review, see Guinan & Giménez 1993; Rucinski 1993). These binaries are known as one of the strong coronal X-ray emission sources. The measured X-ray luminosities are in the range 10^{29}–10^{30} ergs s^{-1}, which are 10^2–10^3 times brighter than that of a typical solar flare. The relatively high X-ray luminosities of this type of binary system are believed to be related to a high level of magnetic activity, caused by dynamo action. It is also believed that the tidal interaction in these binary systems makes the component stars rotate synchronously with their orbital periods ($P_{\rm rot} = P_{\rm orb}$).

VW Cep (HD 197433) is one of the most intensively studied W UMa systems. It is a partial eclipsing contact binary with an orbital period of 0.2783 days. Its component stars have spectral types of $\sim$K0 V and $\sim$G5 V (see Hill 1989 for physical parameters of the stars). One interesting observational feature of this system is that the secondary minimum of the light curve occasionally becomes deeper than the primary minimum. This has been interpreted as the presence of an extended star spot region in the primary, i.e., more massive and cooler, star (Bradstreet & Guinan 1990 and references therein). In the X-ray region, the X-ray spectrum of a 0.1–4.0 keV band is represented by an optically thin thermal plasma model with a combination of two different temperatures, $kT \sim 0.2$–0.6 keV and $kT \sim 1.0$–3.0 keV (Cruddace & Dupree 1984; McGale et al. 1996). Contrary to the optical region, there are no noticeable X-ray eclipses. In addition, an X-ray flare has been detected twice up to now from the source (Vilhu, Caillault, & Heise 1988; McGale et al. 1996), where the flux increases by a factor of ~ 2.5 compared with the quiescent flux level. However, no flare spectrum has been presented and studied in detail so far for this source.

In this paper, we report *ASCA* archival data analysis of the X-ray flare from VW Cep and present a detailed X-ray light curve and an energy spectrum.

2. THE OBSERVATION

ASCA observed VW Cep on 1993 November 5 from 22:37 UT through 9:19 UT on the following day. This span of observation time corresponds to about 1.6 times the orbital period. The *ASCA* satellite (Tanaka, Inoue, & Holt 1994) is equipped with four thin-foil X-ray telescopes that focus X-rays onto four focal plane detectors, two of which are Solid-State Imaging Spectrometers (SIS0, SIS1), and the other two are Gas Imaging Spectrometers (GIS2, GIS3). The telescope has a $\sim 3'$ half-power diameter of the point-spread function. Each of the SISs consists of four CCD chips with a full-width half-maximum energy resolution of $\sim$60–120 eV in the range of 0.4–10 keV, while the GISs have an energy resolution of $\sim$200–600 eV in the range of 0.8–10 keV. The SISs were operated in 1 CCD faint mode for this observation, and the GISs were operated in pulse height mode. The SISs in 1 CCD mode provide a $11' \times 11'$ square field of view, while the GISs give a circular field of view with a diameter of $50'$, regardless of their observational mode.

An X-ray light curve and energy spectrum using the SIS0 and SIS1 detectors are obtained from a rectangular region of $7.'0 \times 7.'4$ centered on the source image. We also obtain the light curve and spectrum by using the GIS2 and GIS3 from the circular region of $6.'2$ radius centered from the source. The background data were obtained from source-

free regions in the same field of view. The background flux was estimated to be much less, from a factor of 3 (GISs) to an order of magnitude (SISs), than the source counting rate. We applied standard data-screening procedures to avoid X-ray contamination from the bright Earth and regions of high particle background (e.g., data were rejected for SISs and GISs when the pointing direction of the telescope was less than 20° and 6° from the Earth's limb, respectively). Hot and flickering pixels were also removed from the SIS data. The net exposure times after the screening were 19,503 s for SIS0 and 27,735 s for GIS2. The average count rate of the screened data was about 0.55 counts s^{-1} and 0.20 counts s^{-1} for SIS0 and GIS2, respectively, after the background subtraction.

3. DATA ANALYSIS AND LIGHT CURVES

We present the X-ray light curves obtained from SIS0 and GIS2 observation in Figure 1. Data from both observations were accumulated in 480 s intervals. The light curves observed with the SIS1 and GIS3 detectors match well with those obtained by using the SIS0 and GIS2, respectively. From the SIS0 data (*upper panel*), one can easily notice a typical pattern of an X-ray flare: a sudden increase of flux from 0.35 counts s^{-1} to about 1 count s^{-1}, followed by a decrease (almost exponentially, except a dip) down to a quiescent level with a timescale of ≈ 6 hr. The quiescent level, indicated by the horizontal dashed line, has an X-ray flux of $F_x = 7.4 \times 10^{-12}$ ergs cm^{-2} s^{-1} in the energy band of 0.4–3.0 keV. This agrees well with the observed flux by Cruddace & Dupree ($F_x = 9.6 \times 10^{-12}$ ergs cm^{-2} s^{-1}) when we extend the energy band to theirs (i.e., 0.1–4.0 keV). The maximum flux level is ~ 2.5 times larger than the quiescent level, and the flux ratio is consistent with the previously detected X-ray flares from this source. The X-ray luminosity of the maximum flux level corresponds to $L_x = 1.2 \times 10^{30}$ ergs s^{-1} (0.4–3.0 keV), assuming the distance to the source to be 23.2 pc. The timescale from the quiescent level to the flare maximum is estimated to be 1–1.5 hr, although it is difficult to measure the onset time of the flare accurately because of the data gap.

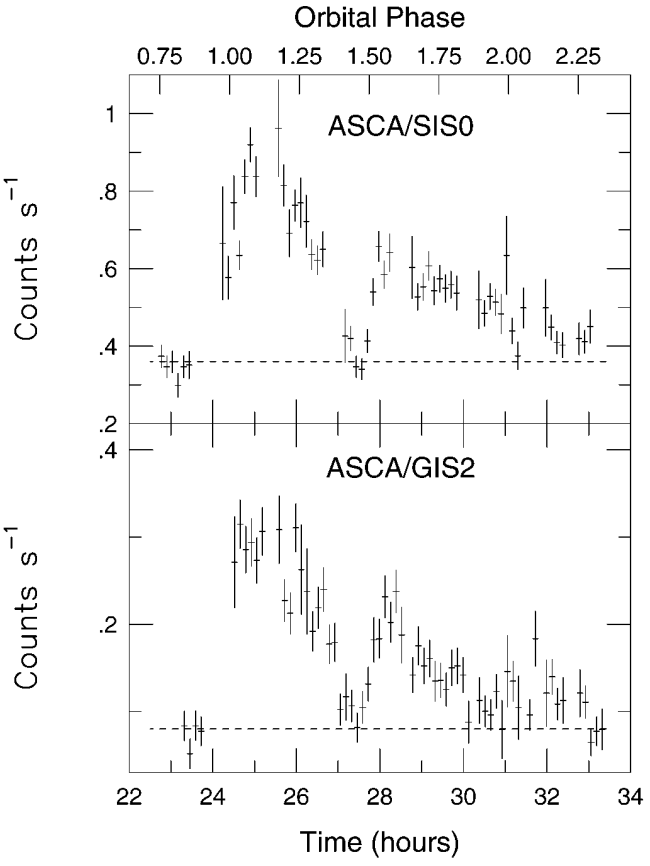

FIG. 1.—X-ray light curves of VW Cep observed with the SIS0 (*upper panel*) and the GIS2 (*lower panel*) detectors. Data were accumulated in 480 s intervals, and the background was subtracted. Horizontal dashed lines indicate a quiescent flux level. The abscissa is hours since 1993 November 5, 0:00 (UT). The numbers at the top of the panel indicate the orbital phase, which is determined from the ephemeris provided by Aluigi et al. (1994).

A dip is apparent around the observation time of 27.5 (MJD = 49,297.1458), particularly in the lower panel of the Figure 1. The dip is recorded in both SIS and GIS data, and we confirm that it is intrinsic to the source. It shows a smooth flux variation, and the duration time takes a few tens minutes for both ingress and egress of the dip. To determine the orbital phase of the dip, we use the ephemeris given in Aluigi, Galli, & Gaspani (1994). Because the orbital period of VW Cep is known to change abruptly (Hill 1989; Arai 1994), it is essential to use the ephemeris determined with the closest data to the X-ray observation. We found that the mid-dip time corresponds to the orbital phase of ~ 0.46. In the case of VW Cep, primary (i.e., deepest) eclipse, which corresponds to phase 0.0 by definition, occurs when the less massive star (the secondary star; $M = 0.25\,M_\odot$ and $R = 0.50\,R_\odot$) is occulted by its larger companion (the primary star; $M = 0.90\,M_\odot$ and $R = 0.93\,R_\odot$). Therefore, it is clear that the flare occurred in the primary star. Although no clear X-ray eclipse has been reported so far for this source, we consider that the flux dip is actually an eclipse, because the orbital phase of the dip coincides well with the secondary eclipse expected from the optical data. We also find that the X-ray flux decreases down to the quiescent level during the mideclipse of the flare. We will discuss in detail about the light curve in § 5.1.

4. SPECTRAL ANALYSIS

It has become possible to study the element abundances of coronal X-ray sources thanks to the high spectral resolution provided by *ASCA*/SIS. However, the source count rates during the present observation are too small to extract a net flare spectrum. Hence, we analyze here the X-ray spectra obtained from the data of the whole light curve. Figure 2 shows the obtained SIS0 and SIS1 spectra. Each spectrum was rebinned to give better data statistics per bin. We truncate data above ~ 3 keV, where there is no significant source photons. The total count rates of the spectra, after the truncation and the background subtraction, are about 0.52 counts s^{-1} for the SIS0 spectrum and 0.44 counts s^{-1} for the SIS1, respectively. One finds that both spectra have many line structures below about 2 keV (where crosses are the data points and histograms are the best-fit model functions). Since we need higher energy resolution to study the spectral structures, we use mainly the SIS data for our analysis.

The results of previous spectral analysis for VW Cep (Cruddace & Dupree 1984; McGale et al. 1996) indicate that its flare spectrum requires a plasma model of two different temperatures. We use the MEKAL model (Mewe, Kaastra, & Liedahl 1995) implemented in the XANADU

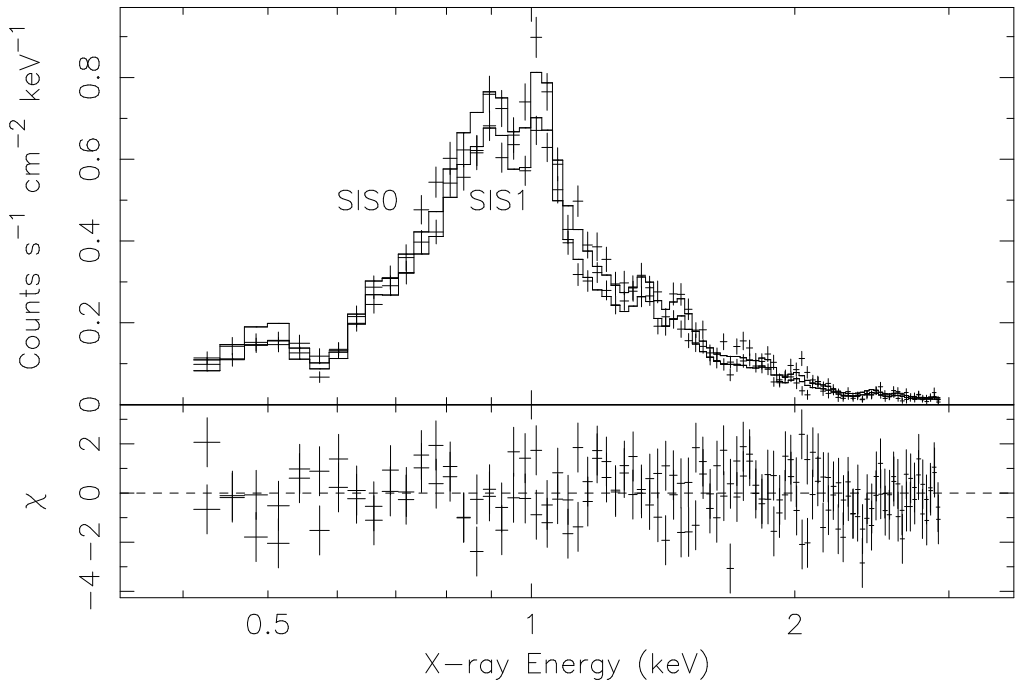

FIG. 2.—X-ray spectra of VW Cep observed with the SIS0 and SIS1 detectors. The SIS spectra were obtained from data of the whole light curve of Fig. 1. We fitted a function of the variable-abundance 2T MEKAL model to both SIS0 and SIS1 spectra simultaneously. The histograms represent the best-fit model function.

XSPEC package as a model emission from an optically thin thermal plasma. The MEKAL model includes line emissions from elements such as He, C, N, O, Ne, Na, Mg, Al, Si, S, Ar, Ca, Fe, and Ni. We use the two-temperature (2T) MEKAL model to fit the energy spectra of SIS with the elemental abundances fixed to the solar photospheric value (Anders & Grevesse 1989). The model function is fitted to both SIS0 and SIS1 spectra simultaneously. However, the fit was not acceptable: the best-fit results in $\chi^2 = 465.6$ with 167 degrees of freedom. We also test a multitemperature model with continuous emission measure distribution and a single-temperature model. However, neither of them improves the result. On the other hand, the 2T MEKAL model gives us a satisfactory fit to the GIS spectra. However, we think this better fit is because of the lower energy resolution of the GIS detectors than SIS. Thus, high-resolution spectra seem to be essential to investigate the spectra of VW Cep. Finally, we try a variable-abundance model. In this fitting, abundances of each element are varied independently, but those of the two MEKAL models are linked together.

TABLE 1

BEST-FIT RESULTS FOR THE VW CEPHEI SPECTRUM

Parameter	Best-Fit Value
kT_1 (keV)	$0.64^{+0.02}_{-0.02}$
EM_1 (10^{52} cm^{-3})	$3.61^{+0.54}_{-0.50}$
kT_2 (keV)	$1.91^{+0.23}_{-0.19}$
EM_2 (10^{52} cm^{-3})	$3.80^{+0.34}_{-0.34}$
Flux[a] (10^{-11} ergs cm^{-2} s^{-1})	$1.22^{+0.01}_{-0.02}$
χ^2/ν	191.6/161
Abundances Relative to Solar Photospheric Abundances	
O	$0.59^{+0.16}_{-0.13}$
Ne	$1.20^{+0.27}_{-0.25}$
Mg	$0.66^{+0.16}_{-0.15}$
Si	$0.50^{+0.14}_{-0.14}$
Fe	$0.27^{+0.05}_{-0.04}$

NOTE.—Errors are at the 90% confidence level for a single parameter.

[a] Calculated in a 0.4–3.0 keV band.

Figure 2 shows the best-fit 2T MEKAL model (*histograms*). The best-fit parameters and their uncertainties measured at the 90% confidence level are listed in Table 1. In the model, interstellar absorption is not considered because there is no significant absorption feature in the spectra. We calculate the upper limit of the absorption column density, which is determined from the uncertainty of the low energy calibration of SIS, not from the data itself. We find that the upper limit is $N_H \sim 2 \times 10^{20}$ cm^{-2}. In the fitting process, the abundances of O, Ne, Mg, Si, and Fe are allowed to vary independently from the solar photospheric values. Abundances of the other elements may not be constrained with the present data mainly because of the limited energy range of the spectra and the small source count rate above 2 keV. According to the recent studies about the element abundances of RS CVn– and Algol-type binaries (Antunes, Nagase, & White 1994; Singh, White, & Drake 1996), the coronal element abundances (e.g., O, Ne, Mg, Si, S, Fe, etc.) are lower by a factor of 2–4 compared with those of the solar photosphere. Therefore, we set the abundances of the other elements to half the solar value. The best-fit parameters in Table 1 imply that the abundances of O, Mg, Si, and Fe are lower than the solar photospheric values by a factor of 2–3, except the relatively high Ne abundance. We also find that the present spectrum can be well explained by the combination of the two different temperatures, $kT = 0.64$ keV and $kT = 1.91$ keV.

5. DISCUSSION

5.1. *Characteristic Parameters of the Flare*

We detected an X-ray flare from the VW Cep system. The rapid rise ($\sim$1–1.5 hr) of X-ray flux and its exponential decay ($\approx$6 hr) shown in Figure 1 are typical of the profile of flares seen in various stars, such as the Sun, flare stars, and late-type binaries, including RS CVn– and Algol-type binaries. Among the stellar X-ray flares observed with *EXOSAT* (Pallavicini 1988; Pallavicini, Tagliaferri, & Stellar 1990), the present flare is very similar to those of Algol (White et al. 1986) and YY Gem in its general profile and the long decay timescale. From the analogy of the profile and the long decay time, the flare of VW Cep is considered to be a "two-ribbon flare" similar to the one observed from the Sun. According to the two-ribbon flare model (Martens & Kuin 1989; see also Haisch, Strong, & Rodono 1991), the long decay time is associated with filament eruptions that may cause a multiple rises and dips in light curves. As was mentioned in the introduction, X-ray flares have been observed twice so far from the VW Cep system. The data of McGale, Pye, & Hodgkin show a large amount of random variability: their light curve shows a high flux near the orbital phase of 0.5 and then the next phase 0.5 shows a low flux. Moreover, in between the orbital phases, there are other high states that last for a short time, less than an hour. These features are different from our results. The present observation shows an exponential flux decrease after reaching the flare peak. Vilhu, Caillault, & Heise also observed a flare by using *EXOSAT*/LE. This flare decays slowly with a timescale of about 3 hr or more, and it shows a very similar pattern to ours. Of course, there exist some differences, including the eclipse pattern, among the observed flare light curves. We think that these differences can be explained by both flaring geometry and classes of flares (e.g., compact and two-ribbon flare). Considering the variety of the light curves, it might be possible to interpret that we actually observed two flares and that the X-ray dip corresponds to the gap between the flares. However, we feel that the dip is the most naturally interpreted as an eclipse, because the dip is observed at just one of the two phases where an eclipse can occur, and the light curves before and after the dip are smoothly connected. Hereafter, we consider the dip as an eclipse.

We estimate the location of the flare from its long duration and the presence of the eclipse. Since the eclipse is overlaid on the flare at the orbital phase of $\sim$0.5, we can easily identify that the flare occurred in the primary star. The decay time of the flare ($\approx$6 hr) is comparable to the orbital period (6.679 hr), implying that the flare is not shadowed by the primary star itself. This is possible if the flare occurred near the pole of the star. However, the visible pole of the primary star cannot be occulted by the secondary star (inclination of the system is $\sim$65°). On the other hand, if we assume that the flare occurred near the invisible pole and if the scale height of the flare is comparable to the extent of the secondary star, such a flare may be occulted by the secondary star, resulting in the present observational results. The characteristic size of the flare is estimated to be comparable to the stellar size of the secondary star (see the following paragraph). Therefore, the flare is thought have occurred near the invisible pole of the primary star.

One of the most important physical parameters of a flare is its size, i.e., the scale height of the magnetic loop of two-ribbon flare. However, no direct measurement has been done. It is quite interesting to note that we have detected the flare eclipse, which not only shows a smooth flux variation but also takes a few tens of minutes for the eclipse ingress and the egress. One may suspect whether it is a flux dip associated with a filament eruption, suggested from the above two-ribbon flare model. However, such features have never been detected in previous long-duration stellar flares. The X-ray flux decreases down to the quiescent level during the mideclipse, implying that the flaring region is entirely occulted by the secondary star. We measure the timescales of the eclipse ingress and egress to be $\sim$40 minutes and $\sim$30 minutes, respectively, determined from a spline fit to the eclipse data shown in Figure 3 (the timescales determined with the SIS data are consistent with those of the GIS data). With only the curve fit, it is difficult to conclude whether the asymmetry is real, because of poor curve fitting to the eclipse ingress. If we use the duration time of the eclipse egress and adopt a combined orbital velocity for the primary and the secondary star of $V_{\rm orb} = 309$ km s^{-1} (Hill 1989), the size of the flaring region would be $\approx 5.5 \times 10^{10}$ cm. This is slightly smaller than the size of the secondary star (7×10^{10} cm) and is consistent to the complete blocking of the flare flux during the mideclipse. In the calculation, we do not consider a rotational effect of the primary star ($V_{\rm rot} = 167$ km s^{-1}) because the effect is negligible for the flare near the pole of the star. The measured size of the flare is comparable to the indirectly measured loop lengths of solar two-ribbon flares ($\sim 10^{10}$ cm; see, e.g., Table 8 of Pallavicini et al. 1990) and an Algol flare ($\sim$2–5 $\times 10^{10}$ cm; White et al. 1986).

The size of the flare is useful to constrain various parameters of the flare. Here we estimate the average electron density of the flare. Between the two temperature components we obtain in the energy spectrum of VW Cep (see Table 1): the hotter component is considered to represent the X-ray emission associated to the flare. If a total of N identical loops of height H are involved in the flare, the emission measure of the flare is represented by

$$\mathrm{EM} \simeq \frac{\pi^4}{8} n_e^2 H^3 (1 + \Gamma) N \alpha^2 , \qquad (1)$$

where n_e is the electron number density, Γ is the ratio of the cross section at the apex and the base of the loop, and α is

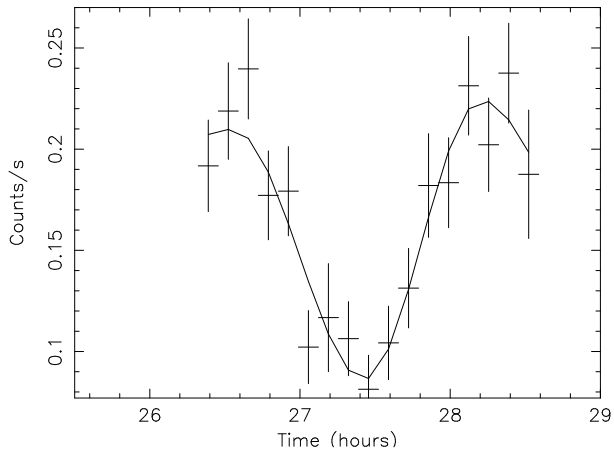

FIG. 3.—Spline fit to the X-ray eclipse of VW Cep. Data were obtained from the GIS2 observation.

the base diameter-to-length ratio (Mewe et al. 1997). The factors Γ and $N\alpha^2$ represent the uncertainty of the flare geometry. Since all these values are poorly known, we use typical values of the Sun ($\Gamma \sim 1$; Feldman et al. 1994) and Algol ($N\alpha^2 \sim 0.004$; van den Oord & Mewe 1989). Based on the emission measure obtained from the spectral fitting (Table 1) and the estimated flare size, we determine the electron density to be $n_e \simeq 5 \times 10^{10}$ cm^{-3}.

Because the plasma is supposed to be confined in the magnetic loop, the magnetic pressure $B^2/8\pi$ should be larger than the gas pressure $2n_e kT$. This condition is used to estimate the lower limit of the magnetic field, and we obtain $B \gtrsim 81$ G. Most of the stellar magnetic field measurements gave values of $\sim 10^3$ G (Saar 1988). Thus, the above estimation is consistent with the idea that the flare plasma is confined in the magnetic loop.

The hot plasma generated near the peak of the flare looses its thermal energy through radiation and/or conduction. Since the decaying timescale is determined from the cooling mechanism, one can identify the cooling mechanism of the flare. The timescale of radiation cooling τ_r is given by

$$\tau_r = \frac{3kT_p}{n_e \Lambda}, \tag{2}$$

where T_p is the peak temperature and Λ is the emissivity of an optically thin plasma. The emissivity is approximated by $\Lambda = 10^{-24.73} T^{1/4}$ ergs cm^3 s^{-1} for temperatures higher than 20 MK (Mewe et al. 1985, 1986). Because we do not know the peak flare temperature, we adopt the average flare temperature of $kT = 1.91$ keV for T_p. This gives a radiation cooling timescale of $\tau_r \simeq 4.0$ hr, which is comparable to the observed flare decay timescale of VW Cep. Another cooling mechanism is conductive energy loss through the footpoints of the loop. The timescale of conduction cooling τ_c is

$$\tau_c = \frac{3n_e kT_p}{\langle E_c \rangle}, \tag{3}$$

where $\langle E_c \rangle$ is the mean conductive energy loss in the loop. By using the formula in van den Oord & Mewe (1989), we determine the conduction cooling timescale to be $\tau_c \simeq 37$ hr. This is much longer than the observed decay timescale of the flare, and thus we conclude that the cooling mechanism would be radiative. Although the present estimation suffers from large uncertainties as a result of the poor time-resolved information of the flare, our result shows that the major cooling mechanism of the VW Cep flare is same as those of Algol (White et al. 1986; van den Oord & Mewe 1989).

5.2. *Results of the Spectral Analysis*

We derive the flare-affected coronal abundances of O, Ne, Mg, Si, and Fe, which are listed in Table 1. Except for the high Ne abundances, the derived abundances are lower by a factor of 2–3 than the solar values. According to the two-ribbon flare model, an enhancement of the coronal element abundances is inevitable. However, as mentioned in § 4, it is difficult to make net flare and quiescent spectra because of the limited data statistics, so that the direct comparison of the element abundances between the quiescent and flare X-ray levels is not possible. We list the element abundances of 44i Bootis in quiescence in Table 2 (Choi & Dotani 1998). 44i Boo is also classified as a W UMa–type binary, and it has a similar spectral type (G2 V + G2) and orbital period (0.2678 days) to the VW Cep system. When the results for VW Cep are compared with those of the 44i Boo system, we find that the element abundances of O, Mg, and Fe are almost the same as those of the 44i Boo system, while the abundances of Ne and Si are larger by a factor of 1.5–2. We think these relatively high Ne and Si abundances, if real, might be related to the flare activity.

TABLE 2

PRELIMINARY RESULTS FOR THE 44i BOOTIS SPECTRUM

Parameter	Best-Fit Value
kT_1 (keV)	$0.65^{+0.02}_{-0.02}$
EM$_1$ (10^{52} cm^{-3})	$2.96^{+0.39}_{-0.43}$
kT_2 (keV)	$1.85^{+0.65}_{-0.36}$
EM$_2$ (10^{52} cm^{-3})	$1.06^{+0.21}_{-0.21}$
Flux[a] (10^{-11} ergs cm^{-2} s^{-1})	$2.31^{+0.36}_{-0.34}$
χ^2/ν	157.3/163
Abundances Relative to Solar Photospheric Abundances	
O	$0.59^{+0.16}_{-0.13}$
Ne	$0.77^{+0.20}_{-0.20}$
Mg	$0.58^{+0.13}_{-0.12}$
Si	$0.27^{+0.12}_{-0.11}$
Fe	$0.24^{+0.04}_{-0.04}$

NOTE.—Errors are at the 90% confidence level for a single parameter.

[a] Calculated in a 0.4–3.0 keV band.

Although the present results need to be taken with care, it is noteworthy that the Ne abundance might be increased in the flare. It is generally believed that abundance enhancement in a solar flare is related to the first ionization potential (FIP) of the element (e.g., McKenzie & Feldman 1992). Compared with high-FIP elements (e.g., O, Ne), the abundances of low-FIP elements (e.g., Si, Mg, Fe) tend to be higher in a solar flare, as well as solar corona, than those in the photosphere. In this respect, it is plausible that the Si abundance of VW Cep during the flare is larger than the quiescent value of 44i Boo. However, a larger Ne abundance poses a problem because Ne has a very high FIP. It is also known that some of the high-FIP elements, such as Ne and Ar, are sometimes anomalously enhanced in a solar flare (Schmelz & Fludra 1993; Fludra & Schmelz 1995). Anomalously high Ne abundance is not explained in the scenario involving only FIP, and thus some other mechanism, such as photoionization (Shemi 1991), is necessary. If the Ne enhancement in the flare of VW Cep is real, it means that the mechanism of the enhancement is similar to that in the Sun despite of the large difference in the flare energetics.

From the spectral analysis of VW Cep, we find that our spectrum can be reproduced by the combination of two different temperatures, $kT = 0.64$ keV and $kT = 1.91$ keV. These temperatures are 2–4 times higher than those determined by McGale et al. (1996). However, the cooler component is consistent with that obtained from the *Einstein* observation by Cruddace & Dupree (1984). Since the spectrum was made with data of the whole light curve, there is no doubt that the cooler component originated in the quiescent X-ray emission. The hotter component represents the flare-averaged temperature, and the value agrees well with a typical flare temperature in the range of $kT = 1$–3 keV (see, e.g., Haisch et al. 1991). The 44i Boo observation shows no flare features, but its spectrum allows a two-temperature model to be fitted acceptably. However, unlike the VW Cep case, the X-ray emission of 44i Boo is domi-

nated by the cooler component (see Table 2); the emission measure of the hotter component is 3 times smaller than that of the cooler component.

6. CONCLUSION

We detect a long-duration flare of ≈ 7.5 hr from the contact binary VW Cep observed with *ASCA*. The flux ratio between the maximum and quiescent levels is about 2.5. Comparison with stellar X-ray flares observed with *EXOSAT* shows that the present flare is very similar to those observed in Algol and YY Gem in overall profile and duration time. A flux dip is detected in the light curve, and it is identified as a flare eclipse occulted by the secondary star. From the long duration and the eclipse, we conclude that the flare occurred near the invisible pole of the primary star. Using a timescale of the eclipse egress of ~ 30 minutes and a combined orbital velocity for the primary and secondary stars of 309 km s^{-1}, the linear size of the flaring region is estimated to be $\approx 5.5 \times 10^{10}$ cm. We note that this estimation is free from any flare models. Using this physical size of the flare, the electron number density of the flare is estimated to be $\sim 5 \times 10^{10}$ cm^{-3}. It is also found that the decay timescale of the flare is mainly determined by radiation cooling. From the spectral analysis of flare data, we find that our spectrum can be reproduced by a variable-abundance plasma model with a combination of two different temperatures, $kT = 0.64$ keV and $kT = 1.91$ keV. The cooler component is consistent with that derived by Cruddace & Dupree (1984) from the *Einstein* observation, and the temperature of the hotter component agrees well with a typical flare temperature in the range of $kT = 1$–3 keV.

We would like to thank Professor Han Cheongho for careful reading of the manuscript. This research has made use of data obtained through the High Energy Astrophysics Science Archive Research Center Online Service, provided by the NASA/Goddard Space Flight Center. Support for this study was provided in part by the research project 97-5600-000 of the Korea Astronomy Observatory.

REFERENCES

Aluigi, M., Galli, G., & Gaspani, A. 1994, IBVS, No. 4117
Anders, E., & Grevesse, N. 1989, Geochim. Cosmochim. Acta, 53, 197
Antunes, A., Nagase, F., & White, N. E. 1994, ApJ, 436, L83
Arai, K. 1994, Exp. Astron., 5, 175
Bradstreet, D. H., & Guinan, E. F. 1990, in Active Close Binaries, ed. C. Ibanoglu (Dordrecht: Kluwer), 467
Carroll, R. W., et al. 1980, ApJ, 235, L77
Choi, C. S., & Dotani, T. 1998, in IAU Symp. 188, The Hot Universe (Dordrecht: Kluwer), in press
Cruddace, R. G., & Dupree, A. K. 1984, ApJ, 277, 263
Feldman, U., et al. 1994, ApJ, 421, 843
Fludra, A., & Schmelz, J. T. 1995, ApJ, 447, 936
Guinan, E. F., & Giménez, A. 1993, in The Realm of Interacting Binary Stars, ed. J. Sahade, G. E. McCluskey, Jr., & Y. Kondo (Dordrecht: Kluwer), 51
Haisch, B., Strong, K. T., & Rodono, M. 1991, ARA&A, 29, 275
Hill, G. 1989, A&A, 218, 141
Martens, P. C. H., & Kuin, N. P. M. 1989, Solar Phys., 122, 263
McGale, P. A., Pye, J. P., & Hodgkin, S. T. 1996, MNRAS, 280, 627
McKenzie, D. L., & Feldman, U. 1992, ApJ, 389, 764
Mewe, R., Gronenschild, E. H. B. M., & van den Oord, G. H. J. 1985, A&AS, 62, 197
Mewe, R., Lemen, J. R., & van den Oord, G. H. J. 1986, A&AS, 65, 511
Mewe, R., Kaastra, J. S., & Liedahl, D. A. 1995, Legacy, 6, 16
Mewe, R., Kaastra, J. S., van den Oord, G. H. J., Vink, J., & Tawara, Y. 1997, A&A, 320, 147
Pallavicini, R. 1988, X-Ray Astronomy with *EXOSAT*, Mem. Soc. Astron. Italiana, 59, 71
Pallavicini, R., Tagliaferri, G., & Stella, L. 1990, A&A, 228, 403
Rucinski, S. M. 1993, in The Realm of Interacting Binary Stars, ed. J. Sahade, G. E. McCluskey, Jr., & Y. Kondo (Dordrecht: Kluwer), 111
Saar, S. H. 1988, ApJ, 324, 441
Schmelz, J. T., & Fludra, A. 1993, Adv. Space Res., 13(9), 325
Shemi, A. 1991, MNRAS, 251, 221
Singh, K. P., White, N. E., & Drake, S. A. 1996, ApJ, 456, 766
Tanaka, Y., Inoue, H., & Holt, S. S. 1994, PASJ, 46, L37
Tsuru, T., Makishima, K., Ohashi, T., Sakao, T., Pye, J. P., Williams, O. R., Barstow, M. A., & Takano, S. 1992, MNRAS, 255, 192
van den Oord, G. H. J., & Mewe, R. 1989, A&A 213, 245
Vilhu, O., Caillault, J.-P., & Heise, J. 1988, ApJ, 330, 922
Vilhu, O., & Heise, J. 1986, ApJ, 311, 937
White, N. E., Culhane, J. L., Parmar, A. N., Kellett, B. J., Kahn, S., van den Oord, G. H. J., & Kuijpers, J. 1986, ApJ, 301, 262